Modeling [11C]yohimbine PET human brain kinetics with test-retest reliability, competition sensitivity studies and search for a suitable reference region

Chloé Laurencin, Sophie Lancelot, Florent Gobert, Jérôme Redouté, Inés Mérida, Thibault Iecker, François Liger, Zacharie Irace, Elise Greusard, Ludovic Lamberet, et al.

NeuroImage 240 (2021) 118328

Contents lists available at ScienceDirect

NeuroImage

journal homepage: www.elsevier.com/locate/neuroimage

Modeling [^{11}C]yohimbine PET human brain kinetics with test-retest reliability, competition sensitivity studies and search for a suitable reference region

Chloé Laurencin[a,b,1], Sophie Lancelot[a,b,c,1], Florent Gobert[b], Jérôme Redouté[c], Inés Mérida[c], Thibault Iecker[c], François Liger[c], Zacharie Irace[c,d], Elise Greusard[b,c], Ludovic Lamberet[b,c], Didier Le Bars[b,c], Nicolas Costes[a,c,1], Bénédicte Ballanger[a,1,*]

[a] Lyon Neuroscience Research Center (CRNL), INSERM U1028, CNRS UMR5292, University Lyon 1, Lyon F-69000, France
[b] Pierre Wertheimer Neurological Hospital, Hospices Civils de Lyon (HCL), Lyon, France
[c] CERMEP, Lyon, France
[d] Siemens-Healthcare, SAS, Saint-Denis, France

ARTICLE INFO

Keywords:
[^{11}C]yohimbine
α2-adrenoceptors
Positron emission tomography
Human brain
Compartmental modeling

ABSTRACT

Previous work introduced the [^{11}C]yohimbine as a suitable ligand of central α2-adrenoreceptors (α2-ARs) for PET imaging. However, reproducibility of [^{11}C]yohimbine PET measurements in healthy humans estimated with a simplified modeling method with reference region, as well as sensitivity of [^{11}C]yohimbine to noradrenergic competition were not evaluated. The objectives of the present study were therefore to fill this gap. *Methods:* Thirteen healthy humans underwent two [^{11}C]yohimbine 90-minute dynamic scans performed on a PET-MRI scanner. Seven had arterial blood sampling with metabolite assessment and plasmatic yohimbine free fraction evaluation at the first scan to have arterial input function and test appropriate kinetic modeling. The second scan was a simple retest for 6 subjects to evaluate the test-retest reproducibility. For the remaining 7 subjects the second scan was a challenge study with the administration of a single oral dose of 150 µg of clonidine 90 min before the PET scan. Parametric images of α2-ARs distribution volume ratios (DVR) were generated with two non-invasive models: Logan graphical analysis with Reference (*LREF*) and Simplified Reference Tissue Method (*SRTM*). Three reference regions (cerebellum white matter (CERWM), frontal white matter (FLWM), and corpus callosum (CC)) were tested. *Results:* We showed high test-retest reproducibility of DVR estimation with *LREF* and *SRTM* regardless of reference region (CC, CERWM, FLWM). The best fit was obtained with $SRTM_{CC}$ (r^2=0.94). Test-retest showed that the $SRTM_{CC}$ is highly reproducible (mean ICC>0.7), with a slight bias (-1.8%), whereas $SRTM_{CERWM}$ had lower bias (-0.1%), and excellent ICC (mean>0.8). Using $SRTM_{CC}$, regional changes have been observed after clonidine administration with a significant increase reported in the amygdala and striatum as well as in several posterior cortical areas as revealed with the voxel-based analysis. *Conclusion:* The results add experimental support for the suitability of [^{11}C]yohimbine PET in the quantitative assessment of α2-ARs occupancy in vivo in the human brain.

Trial registration EudraCT 2018-000380-82

1. Introduction

Investigations of the noradrenergic system function in the brain have mainly emerged from animal studies so far. Indeed, the lack of suitable imaging tools has hampered its understanding in human. Nevertheless, we now have the possibility to overcome this difficulty as in vivo imaging of the noradrenergic system has recently become feasible with the development of a novel PET radiotracer: [^{11}C]yohimbine (Nahimi et al., 2015). Yohimbine is an antagonist of the α2-adrenoreceptors (α2-ARs) and a partial agonist of the 5-HT_{1A} receptors (Millan et al., 2000). The radiotracer [^{11}C]yohimbine binds with high selectivity to all α2-ARs subtypes (Jakobsen et al., 2006). This represents a great opportunity

* Corresponding author at: CRNL - INSERM U1028 - CNRS UMR5292, UCBL, CH Le Vinatier – Bât. 462 – Neurocampus, 95 boulevard Pinel, Bron Cedex 69675, France
E-mail address: benedicte.ballanger@cnrs.fr (B. Ballanger).
[1] These authors contributed equally to this work

https://doi.org/10.1016/j.neuroimage.2021.118328.
Received 16 February 2021; Received in revised form 20 May 2021; Accepted 30 June 2021
Available online 3 July 2021.

towards the collection of missing data in the living human brain by direct quantification of regional α2-ARs availability. Indeed, α2-ARs play a key role in regulating noradrenergic neurotransmission (Szabadi, 2013) as altered noradrenergic transmission with specific loss of α2-ARs is currently theorized to play a critical role in both symptoms and progression of some neurodegenerative and mood disorders (Marien et al., 2004; Ordway et al., 2003). Human in vivo imaging of α2-ARs is therefore essential. Previous work showed that [^{11}C]yohimbine PET tissue data can be described by a 1 tissue compartment (1-TCM), and α2-ARs binding potential can be estimated using the corpus callosum (CC) as reference tissue (Nahimi et al., 2015). Simplified Reference tissue methods (*SRTM*) have been widely used to estimate neuroreceptor binding potential because they eliminate the invasive arterial input function (AIF) step. However, reproducibility of non-displaceable binding potential (BP_{ND}) in healthy humans, as well as displaceability with an α2-ARs agonist, were not evaluated. Yet, demonstration of a reproducible [^{11}C]yohimbine PET outcome measure is critical and preliminary to accurately determine the clinical significance of pharmacologic or pathophysiologic α2-ARs changes.

The objectives of the present study were therefore (1) to identify an optimal [^{11}C]yohimbine PET full kinetic modeling with AIF, (2) assess the validity of non-invasive kinetic modeling, (3) identify the best reference region, (4) estimate the reproducibility of [^{11}C]yohimbine PET measurements with test-retest scans and (5) examine the sensitivity of [^{11}C]yohimbine with a noradrenergic pharmacological competition using acute administration of clonidine, a drug known to decrease NA release through pre-synaptic α2-ARs activation.

2. Materials and methods

All procedures performed in this study were in accordance with the ethical standards of the institutional and national research committee and with the principles of the 1964 Declaration of Helsinki and its later amendments or comparable ethical standards. The study was approved by the Ethics Committee of Sud Mediterranée III (EudraCT: 2018–000380–82) and pre-registered before being conducted on the ClinicalTrials.gov database under the trial record number NCT03520543. The subjects gave written informed consent to participate in the study.

2.1. Participants

Over sixteen healthy men included, two were discontinued, and fourteen completed the study. The mean age was 25 years old (standard deviation, SD, 3 years) and the mean weight was 74. 4 ± 7.2 kg (range, 63–87). All subjects were free of medical or neuropsychiatric illness and none of them were smokers or under medication. Each subject underwent two [^{11}C]yohimbine PET scans separated by an interval of 7 to 21 days. For the first scan (test), an arterial catheter was inserted into the radial artery after completion of the Allen test and infiltration of the skin with 1% lidocaine. For the second scan, 7 subjects had a repeated baseline PET (retest), and 7 other subjects had a second PET 74 ± 11 min after administration of a 150 µg oral dose of clonidine (challenge). For all subjects, this second scan was performed without blood sampling. Subjects were also genotyped for the cytochrome P450 (CYP) system with regard to the CYP2D6 isoform, as this latter is involved in the metabolism of yohimbine in the liver, yielding two metabolites that may have some action at α2-ARs (Le Corre et al., 1999).

2.2. PET procedures

[^{11}C]yohimbine was synthesized as previously described (Jakobsen et al., 2006). The radiochemical purities of syntheses used for the study were greater than 95%, with corresponding molar activities of 53.4 ± 16.4 GBq/µmol at the end of synthesis.

All subjects received an intravenous bolus injection of 370 MBq ± 10% of [^{11}C]yohimbine (Table 1). List-mode PET data were acquired, during 90 min from the injection of the tracer, simultaneously with 3T MRI data (Dixon T1, anatomic MPRAGE T1, veinous and arterial TOF), on a Siemens mMR Biograph system.

2.3. Input function measurement

AIF (*Ca*) and metabolite levels in the plasma were measured from 25 heparinized arterial blood samples manually collected with the following timing: every 5 s for the first minute, every 10 s until second minute, and at times 5, 10, 30, 45, 60, and 90 min post-injection. Eight whole blood aliquots (100 µL), at times of 1, 2, 5, 10, 30, 45, 60, and 90 min post injection, were counted in gamma counter (Perkin-Elmer) to evaluate whole blood to plasma ratio (f_{wb}). Twenty-five blood samples were centrifuged for 3 min (4000 g) and plasma aliquots (100 µL) were counted in gamma counter to measure uncorrected plasma curve (*Cp*). For metabolite analysis, other plasma aliquots were filtrated using a 0.45 µm membrane filter. Two hundred microlliliter plasma filtrates were injected in HPLC system with a C8 CAPCELL PAK MF column (Osaka Soda). Fractions were collected and counted for radioactivity in gamma counter. The activity of [^{11}C]yohimbine was divided by the total activity recovered from the gamma counter to give the plasma parent fraction of unmetabolized [^{11}C]yohimbine (PPf). Plasma-free fraction of [^{11}C]yohimbine freely diffusible to tissue (*fp*) was measured by ultrafiltration at 1, 2, 5, 10, 30, 45, 60, and 90 min post-injection as previously described (Moore et al., 2003). Arterial blood samples were centrifuged, and 1 mL of plasma was placed in ultracentrifugation devices (Centrifree®, Millipore) and spun for 10 min at 2000 g. One hundred microlliliter aliquots of whole plasma and ultrafiltrate were counted in gamma counter. After counting, all samples were weighed, and counts were corrected. The *fp* was determined from the ratio of concentrations in the ultrafiltrate and whole plasma. AIF was the plasma curve corrected from the plasma parent fraction curve $AIF(t) = PPf(t).Cp(t)$. The whole blood curve was determined by the mean f_{wb} and the plasma curve $Cwb(t) = f_{wb}.Cp(t)$.

2.4. Image processing

Raw PET data were motion corrected (Reilhac et al., 2018), then rebinned into 24-time frames (variable length frames, 8 × 15 s, 3 × 60 s, 5 × 120 s, 1 × 300 s, 7 × 600 s) sinograms for dynamic reconstruction. Images were reconstructed using 3D ordinary Poisson-ordered subsets expectation maximization (OP-OSEM 3D), incorporating the system point spread function using 3 iterations of 21 subsets. Sinograms were corrected for scatter, randoms, normalization and attenuation (Mérida et al., 2017). Reconstructions were performed with a zoom of 2, yielding a voxel size of 2.03 × 2.03 × 2.08 mm^3 in a matrix of 172 × 172 voxels with a 4 mm 3D post-reconstruction gaussian filtering. The mean PET image of the session 2 was coregistered (rigid transform) onto the mean PET image of the session 1. Individual MRI T1 of the first session was normalized to the MNI space (Montreal Neurological Institute template of the International Consortium for Brain Mapping Project) with the *Segment* function of SPM 12 (Ashburner and Friston, 2005). Labeling of the structural brain regions was performed using the multi-atlas propagation with enhanced registration (MAPER) methodology (Heckemann et al., 2010), and the 83-region Hammersmith atlas (Hammers et al., 2003). After projection of the atlas onto the two sessions, regional time activity curves (TAC) were extracted for a selection of brain regions including the amygdala, cerebellum, corpus

Table 1
Details of the CYP2D6 status for each subject and Injected Radioactivity Dose, Molecular Activity, Free fraction in plasma (*fp*), Plasma to whole blood fraction (f_{wb}).

Subject	Gaedigk Activity Score	Scan 1 Test				Scan 2 ReTest		Scan 2 Challenge	
		MBq	GBq/μmol	*fp* (%)	f_{wb} (%)	MBq	GBq/μmol	MBq	GBq/μmol
1	1.5 (E)	319	27	–	70.3	*Not available*			
2	1.5 (E)	351	24	7.8	66.3	355	21		
3*	1 (I)	376	22	6.8	66.3		366	30	
4*	2 (E)	376	12	10.5	71.3			355	22
5	1 (I)	351	31	7.6	59.8	414	45		
6*	1.5 (E)	355	44	8.0	62.9			373	33
7*	2 (E)	374	19	6.3	66.4			362	34
8	1 (I)	362	36	–	–			393	14
9*	1 (I)	363	42	8.0	66.1	370	29		
10	1 (I)	367	25	7.4	66.5	367	24		
11	1.5 (E)	341	33	8.7	63.2			361	24
12	1 (I)	384	31	–	–	385	27		
13*	2 (E)	351	28	11.3	69.9			381	20
14*	1.25 (E)	355	48	10.7	64.4	357	39		
Mean±SD		*359±17*	*30± 10*	*8.5± 1.7*	*66.1 ± 3.3*	*375± 22*	*31± 9*	*370± 13*	*25± 7*

*subjects included in the kinetic modeling analysis. CYP2D6 activity score calculated according to Gaedigk's method (2008) (I and *E* = Intermediate and Extensive metabolizers respectively).

callosum, frontal lobe, gyrus cinguli, insula, occipital lobe, parietal lobe, striatum, temporal lobe, and thalamus.

2.5. Kinetic modeling

Modeling of the PET TAC was performed with the AIF corrected for metabolite and plasma free fraction using the Turku PET center utilities library (*TPCCLIB*, https://gitlab.utu.fi/vesoik/tpcclib). Invasive models including the 1-TCM (*fitk2*), the 2-TCM (*fitk4),* and the Logan graphical analysis (LGA) (Logan, 2000) were used to estimate the volume of distribution (V_T, mL.g^{-1}) across regions. Fitting accuracy was evaluated with the Akaike information criteria (AIC) (Akaike, 1974). Reference tissue modeling techniques were also evaluated using *SRTM* (Lammertsma and Hume, 1996) and the non-invasive Logan reference tissue model (*LREF)* (Logan, 2000). The CC was chosen as reference region based on the recommendations of previous work (Nahimi et al., 2015). In addition, the cerebellar white matter (CERWM) and the frontal lobe white matter (FLWM) were also tested as potential reference tissue because white matter has previously been proposed to represent a region of non-specific binding (Landau et al., 2012). The distribution volume ratio (DVR) was the parameter of interest of the simplified modeling techniques: DVR_{SRTM}, DVR_{LREF}, and $DVR_{1\text{-}TCM}$ (DVR computed as the ratio of the V_T of the target region to the V_T in the reference region, derived from the 1-TCM with AIF).

Reference tissue modeling was also performed at the voxel level to compute intra-cerebral DVR parametric maps with *SRTM* (Gunn et al., 1997) and with *LREF* (Varga and Szabo, 2002). DVR parametric images were then transformed from the subject's space to the MNI space using the nonlinear deformation fields derived from the spatial normalization of the individual's MR image. Finally, normalized parametric images were smoothed using an $8 \times 8 \times 8$-mm^3 full width at half maximum isotropic gaussian kernel to account for the interindividual anatomy variability, normalization uncertainties, and to improve the sensitivity of the SPM analysis. Additionally, regional mean DVR values were computed from the parametric maps in the subject's space.

2.6. Test-retest reproducibility study

2.6.1. Bias and variability

The test-retest bias was calculated as the difference between the test and retest DVRs, divided by the mean of the test and retest values, and the variability as the SD of the bias. These parameters were expressed as percentage.

2.6.2. Reliability

The reliability of the measurements was assessed by the intraclass correlation coefficient (ICC) calculated as (BSMSS-WSMSS)/(BSMSS+WSMSS) where BSMSS is the mean sum of square between subjects and WSMSS is the mean sum of square within subjects (Shrout and Fleiss, 1979). This statistic estimates the relative contributions of between- and within-subject variability and assumes values from −1 (i.e., BSMSS = 0) to 1 (identity between test and retest, i.e., WSMSS = 0).

2.7. Test-challenge study

Clonidine is highly selective and exerts potent agonistic effects at pre-synaptic α2-ARs (Delaville et al., 2011). Regional changes induced by the challenge with clonidine were computed as the relative difference of DVR between scans in selected ROIs, expressed as percentage. Binding changes were also observed at the voxel level.

2.8. Statistical analysis

Statistical analysis was performed using Rstudio (https://github.com/rstudio/rstudio). Paired Student's t-tests were used to test for differences in the injected dose and molar activity of the [^{11}C]yohimbine between Scan 1 and Scan 2 and also applied to test whether DVRs after retest or clonidine challenge significantly differed from baseline condition. Results with $p<0.05$ were considered statistically significant. SPM12 was used for voxel-wise comparison with spatially normalized smoothed DVR images. Statistical parametric maps of the t statistic were computed with a threshold of $p<0.05$ uncorrected at the voxel level and an extent voxels threshold the "*Expected number of voxel per cluster*". Significant clusters were selected at a corrected cluster level of $p<0.05$ ("*False discovery rate*") (Poline et al., 1997).

3. Results

3.1. Subject demographics

In total, over the fourteen subjects scanned, only thirteen completed the study according to the protocol. One subject's retest scan (subject 1) was not evaluated because of PET camera malfunction during the acquisition and was excluded from the test-retest analysis. Additionally, over the thirteen subjects, two subjects did not have arterial sampling in scan 1 but completed the study. For three subjects, the metabolite data were non-exploitable. At the end, for the modeling study, seven

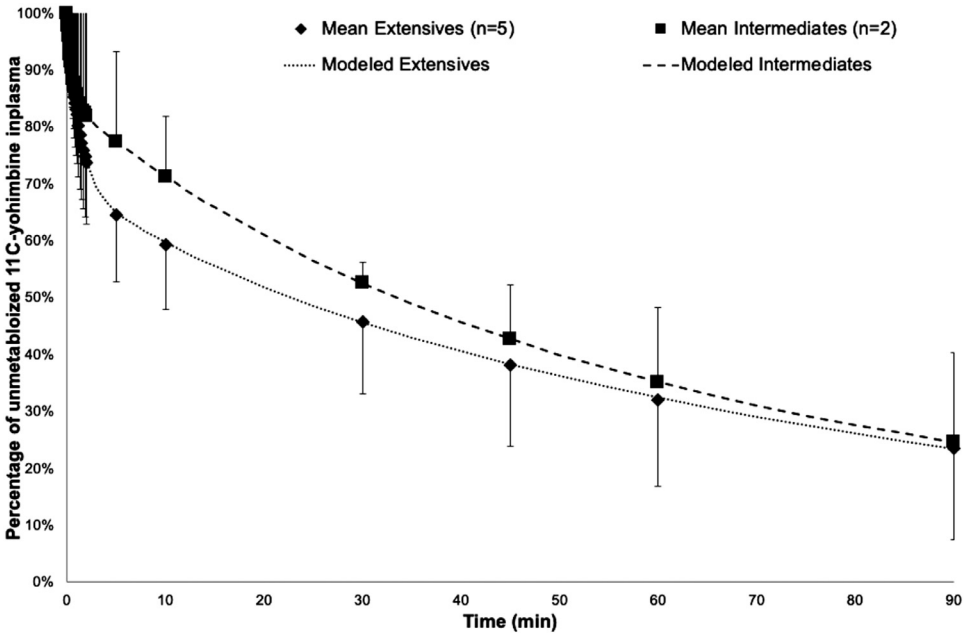

Fig. 1. Plasma parent fraction (PPf) of unmetabolized [^{11}C]yohimbine calculated for the group of intermediate metabolizers and the group of extensive metabolizers (mean and SD across subjects in each group).

datasets were available (PET scan, AIF, metabolite function and free fraction), for the test-retest, six datasets were available (six subjects, two PET scans), and for the test-challenge study, seven datasets were available (seven subjects, two PET scans) (Table 1). Mean age for both groups was identical (25±4 years old for the test-retest group and 25±2 for the test-challenge group).

3.2. Modeling study

Fig. 1 shows metabolization curve (mean and SD plasma parent fractions across subjects) and its modeling depending on the CYP2D6 activity. The best modeling curve of the mean plasma parent fraction curve was a 3-exponentials model:

$$PPf\ (t) = A1.e^{\left(-\frac{t}{T1}\right)} + A2.e^{\left(-\frac{t}{T2}\right)} + A3.e^{\left(-\frac{t}{T3}\right)}$$

with A1= 0.16, T_1 = 0.41, A2= 0.27, T_2 = 21.45, and A3= 0.57, T_3 = 68.97 for the group of intermediate metabolizers, and with A1= 0.30, T_1 = 0.88, A2= 0.09, T_2 = 11.49, and A3= 0.61, T_3 = 65.77 for the group of extensive metabolizers.

Free plasma fraction was constant over time and had a mean value of 8.5 ± 1.7%. Note that intermediate metabolizers presented mean lower *fp* values compared to extensive metabolizers (7.4 ± 0.5% and 9.1 ± 1.8%, respectively) not statistically significant ($W = 22$, $p = 0.16$). Whole blood to plasma ratio was constant over time with a mean value of 66.1 ± 3.3% (Table 1) without significant differences between both types of genotypes ($W = 21$, $p = 0.46$). Fig. 2 shows an example of AIF corrected for metabolites and whole blood concentration curve for one subject with intermediate CYP2D6 activity and one subject with extensive profile.

Overall, the Akaike information (AIC) showed slightly lower values for the 2-TCM (225 ± 21) compared to the 1-TCM (244 ± 18) approach, indicating better fits for the 2-TCM. However, as previously highlighted (Nahimi et al., 2015), the 1-TCM approach is much more robust and produced less non-physiological estimates of the kinetic parameters. Accordingly, the 1-TCM was judged as the most appropriate model for analysis of [^{11}C]yohimbine imaging data. Kinetic parameters and V_T using 1-TCM and LGA in the investigated brain regions are reported in Table 2. The V_T were higher in almost all the cortical regions (>0.4). Lower V_T were observed in the cerebellum and the striatum (<0.35) as well as in the three potential reference tissues (CERWM, CC, FLWM). Although, the regression between V_T values computed by the 1-TCM model and V_T values computed with LGA were extremely well correlated ($V_{T\_LGA} = 0.99^{*}V_{T\_1\text{-}TCM} + 0.04$; $r^2 = 0.98$; $p<0.001$), this latter model slightly but significantly overestimated V_T in all regions compared to 1-TCM ($p < 0.0002$).

3.3. Model with tissue reference regions

Regression of DVR_{LREF} and DVR_{SRTM} to $DVR_{1\text{-}TCM}$ for the three tested reference regions are shown in Table 3. Regression coefficients were over 0.8 for all regressions, with the best fit obtained for $SRTM_{CC}$ (0.94). Regression slopes were close to 1 for both methods (ranging from 0.81 for $SRTM_{CERWM}$ to 1.13 for $SRTM_{CC}$). Intercepts ranged from 0.03 ($SRTM_{CC}$) to 0.24 ($SRTM_{CERWM}$).

3.4. Test-retest study

There were no significant differences between test and retest scans in neither the amount of radioactivity injected (MBq mean ± SD: Scan 1: 361.8 ± 12.6; Scan 2: 374.7 ± 22.1; *Student_t*= −1.3; $p = 0.26$) nor the molar activity of [^{11}C]yohimbine (GBq/μmol mean ± SD: Scan 1: 33.5 ± 9.5; Scan 2: 30.8 ± 9.2; *Student_t* = 0.71; $p = 0.51$). The biases, variabilities and ICC values of the [^{11}C]yohimbine binding parameters are presented in Table 3 (right part) for both compartmental models with the three potential reference tissues. Reliability was very good (> 0.74) for both models using either the CC or the CERWM as reference region, while it was acceptable when using the FLWM (around 0.5). The mean values of bias were low (< 2%) for all models, and the average variability ranged from 3.8% for the $SRTM_{CERWM}$ to 6.3% for the $LREF_{CC}$ model. Test and retest DVR values were highly correlated (R^2 > 0.98). Test-retest performance based on averaged values across subjects are presented in detail, region by region, in Table 4 for the most reproducible methods, namely the *LREF* and the *SRTM* with CC and CERWM as reference regions. Using the CC, the test-retest DVR reliability was moderate to high, ranging from 0.67 (gyrus cinguli) to 0.93 (cerebellum) with the *LREF* and from 0.52 (striatum) to 0.98 (cerebellum) with the *SRTM*. Using the CERWM, the test-retest DVR reliability was also moderate to high, ranging from 0.59 (frontal lobe) to 0.92 (amygdala) with the *LREF* and from 0.70 (cerebellum) to 0.92 (amygdala) with the *SRTM*. The test-retest DVR variability was excellent ranging from 2.6% (cerebellum) to 7.1% (insula) using the *SRTM* with CC, while this

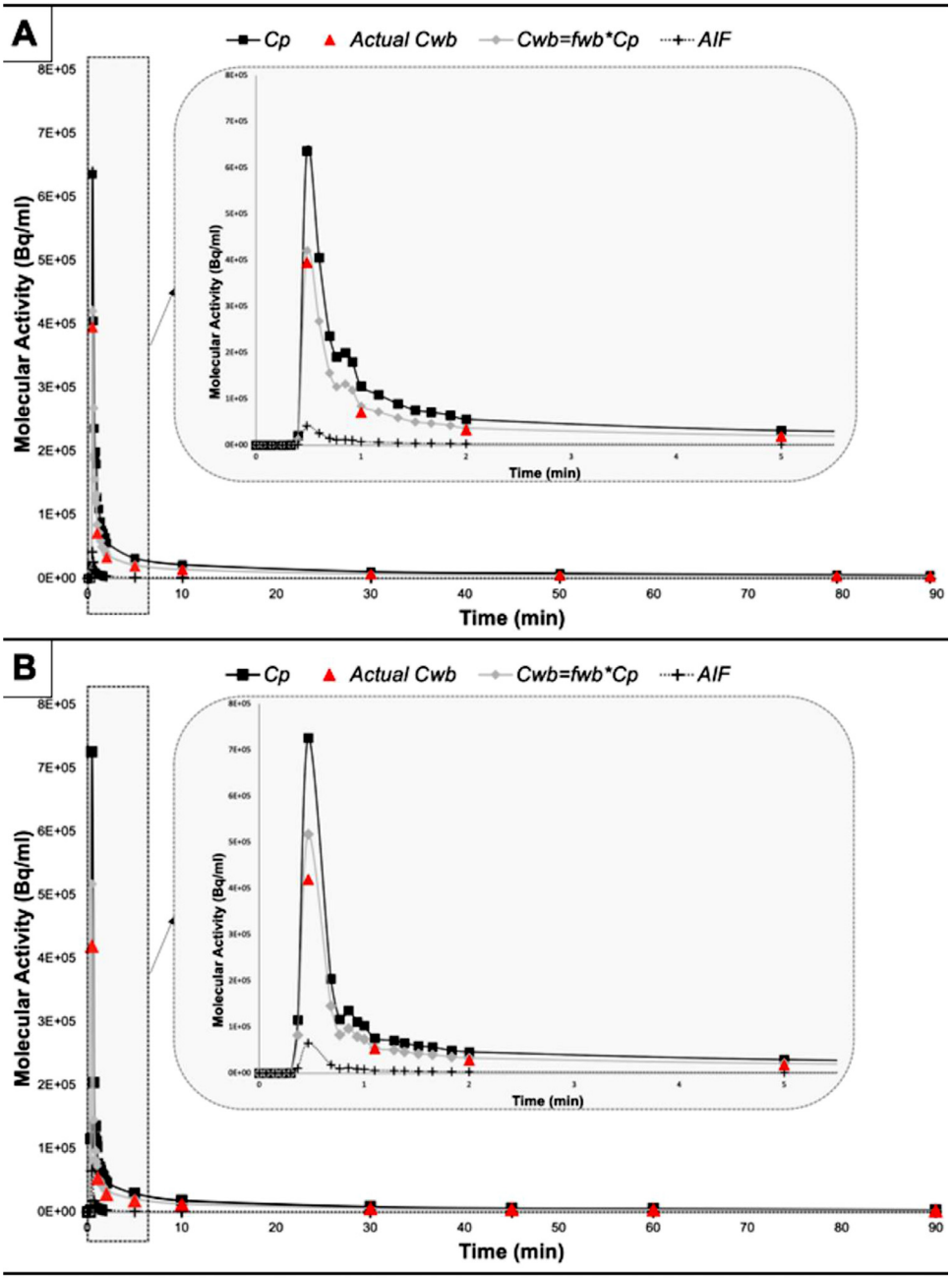

Fig. 2. Illustration of arterial input function (AIF), whole blood plasma (C_{wb}), uncorrected plasma (*Cp*) curves for one intermediate metabolizer subject (Part A) and one extensive metabolizer (part B). f_{wb}: plasma to whole blood fraction.

Table 2
Kinetic parameters and V_T estimated with 1-TCM and LGA in 7 healthy volunteers.

Regions	1-TCM V_b (%)	LGA K_1 (mL/cm^3/min)	k_2 (min^{-1})	V_T (mL/cm^3)	V_T (mL/cm^3)
Amygdala	2.3 ± 0.8	0.007 ± 0.002	0.019 ± 0.004	0.39 ± 0.08	0.41 ± 0.08
Cerebellum	2.3 ± 0.9	0.010 ± 0.003	0.029 ± 0.004	0.34 ± 0.07	0.39 ± 0.07
Frontal Lobe	1.7 ± 0.8	0.011 ± 0.003	0.025 ± 0.004	0.42 ± 0.10	0.45 ± 0.10
Gyrus Cinguli	2.3 ± 0.8	0.011 ± 0.003	0.023 ± 0.005	0.45 ± 0.10	0.49 ± 0.10
Insula	2.4 ± 0.8	0.009 ± 0.003	0.022 ± 0.004	0.41 ± 0.10	0.45 ± 0.09
Occipital Lobe	2.0 ± 0.9	0.011 ± 0.003	0.025 ± 0.004	0.42 ± 0.10	0.46 ± 0.10
Parietal Lobe	2.0 ± 0.8	0.011 ± 0.003	0.025 ± 0.004	0.42 ± 0.10	0.46 ± 0.10
Striatum	1.6 ± 0.7	0.010 ± 0.003	0.029 ± 0.004	0.34 ± 0.09	0.37 ± 0.08
Temporal Lobe	1.9 ± 0.8	0.009 ± 0.003	0.023 ± 0.004	0.41 ± 0.10	0.45± 0.10
Thalamus	2.3 ± 0.9	0.010 ± 0.003	0.024 ± 0.005	0.42 ± 0.09	0.46 ± 0.09
Cerebellum White Matter (CERWM)	1.5 ± 0.6	0.008 ± 0.002	0.025 ± 0.004	0.31 ± 0.06	0.35 ± 0.06
Corpus Callosum (CC)	1.5 ± 0.6	0.005 ± 0.001	0.015 ± 0.002	0.32 ± 0.07	0.36 ± 0.07
Frontal Lobe White Matter (FLWM)	1.1 ± 0.5	0.007 ± 0.002	0.019 ± 0.003	0.34 ± 0.08	0.36 ± 0.08

Data are presented as mean values (± SD).

Table 3
Validation and reproducibility of the distribution volume ratio (DVR) computed with models with reference region, against gold standard 1-TCM model with AIF.

		Mean Regression parameters over $DVR_{1\text{-}TCM}$			Mean Test-Retest reproducibility parameters					
		Slope	Intercept	R^2	ICC	Bias (%)	VAR (%)	Slope	Intercept	R^2
DVR_{LREF}	CC	1.07 ± 0.13	0.16 ± 0.16	0.84 ± 0.06	0.75 ± 0.08	−1.2	6.3	0.96	0.05	0.99
	CERWM	0.94 ± 0.14	0.06 ± 0.15	0.81 ± 0.07	0.75 ± 0.10	0.8	4.1	0.97	0.05	0.99
	FLWM	0.98 ± 0.12	0.14 ± 0.14	0.82 ± 0.07	0.56 ± 0.22	0.7	4.3	0.97	0.05	0.99
DVR_{SRTM}	CC	1.13 ± 0.05	0.03 ± 0.08	0.94 ± 0.04	0.74 ± 0.12	−1.8	4.9	0.94	0.06	0.98
	CERWM	0.81 ± 0.09	0.24 ± 0.10	0.85 ± 0.07	0.82 ± 0.07	−0.1	3.8	0.93	0.09	0.98
	FLWM	0.94 ± 0.08	0.14 ± 0.10	0.92 ± 0.05	0.45 ± 0.31	−0.1	4.2	0.95	0.06	0.98

Data are presented as mean values (± SD).

Table 4
Mean regional DVR test-retest reproducibility and test-challenge variations.

		Test-Retest Study					Challenge Study		
Model	Structures	DVR Test	DVR Retest	ICC	Bias (%)	VAR (%)	DVR Test	DVR Challenge	Change (%)
$LREF_{CC}$	Amygdala	1.23 ± 0.08	1.23 ± 0.08	0.71	−0.14	4.82	1.30 ± 0.16	1.36 ± 0.13	5.2 ± 5.9
	Cerebellum	1.30 ± 0.15	1.28 ± 0.20	0.93	−1.88	4.74	1.36 ± 0.19	1.39 ± 0.13	2.5 ± 8.3
	Frontal Lobe	1.49 ± 0.13	1.47 ± 0.17	0.70	−1.57	7.94	1.61 ± 0.14	1.56 ± 0.15	−2.5 ± 5.1
	Gyrus Cinguli	1.56 ± 0.13	1.54 ± 0.16	0.67	−1.58	7.80	1.64 ± 0.15	1.63 ± 0.15	−0.7 ± 3.0
	Insula	1.41 ± 0.14	1.39 ± 0.13	0.73	−1.55	6.97	1.47 ± 0.13	1.48 ± 0.13	0.5 ± 4.5
	Occipital Lobe	1.47 ± 0.10	1.44 ± 0.14	0.78	−2.23	5.44	1.53 ± 0.18	1.55 ± 0.15	1.7 ± 6.7
	Parietal Lobe	1.49 ± 0.11	1.48 ± 0.16	0.68	−0.90	7.21	1.58 ± 0.14	1.56 ± 0.15	−1.1 ± 3.4
	Striatum	1.27 ± 0.11	1.26 ± 0.11	0.68	−0.57	7.10	1.31 ± 0.10	1.32 ± 0.11	1.0 ± 3.6
	Temporal Lobe	1.40 ± 0.12	1.37 ± 0.14	0.80	−1.80	5.76	1.46 ± 0.15	1.48 ± 0.14	1.4 ± 4.6
	Thalamus	1.43 ± 0.13	1.43 ± 0.14	0.83	0.01	5.32	1.55 ± 0.19	1.55 ± 0.17	0.6 ± 3.2
$SRTM_{CC}$	Amygdala	1.23 ± 0.06	1.21 ± 0.06	0.82	−1.38	2.72	**1.28 ± 0.16**	**1.36 ± 0.12**	6.3 ± 7.9
	Cerebellum	1.14 ± 0.14	1.13 ± 0.15	0.98	−1.56	2.60	1.19 ± 0.16	1.23 ± 0.13	4.5 ± 9.7
	Frontal Lobe	1.48 ± 0.11	1.45 ± 0.11	0.79	−1.90	5.10	1.58 ± 0.14	1.57 ± 0.14	−0.9 ± 6.1
	Gyrus Cinguli	**1.54 ± 0.11**	**1.51 ± 0.12**	0.73	−2.37	5.89	1.61 ± 0.15	1.62 ± 0.14	0.4 ± 4.4
	Insula	1.38 ± 0.13	1.33 ± 0.10	0.64	−3.37	7.13	1.43 ± 0.12	1.44 ± 0.11	0.8 ± 5.2
	Occipital Lobe	**1.44 ± 0.08**	**1.39 ± 0.09**	0.79	−3.64	4.02	1.48 ± 0.17	1.51 ± 0.14	2.7 ± 8.7
	Parietal Lobe	1.45 ± 0.09	1.44 ± 0.11	0.68	−0.85	5.35	1.53 ± 0.12	1.53 ± 0.14	0.4 ± 6.4
	Striatum	1.19 ± 0.08	1.19 ± 0.08	0.52	−0.33	6.21	**1.20 ± 0.08**	**1.25 ± 0.11**	4.4 ± 6.5
	Temporal Lobe	**1.39 ± 0.10**	**1.35 ± 0.11**	0.81	−3.16	4.45	1.44 ± 0.14	1.48 ± 0.14	2.4 ± 6.0
	Thalamus	1.36 ± 0.10	1.37 ± 0.10	0.67	0.23	5.32	1.45 ± 0.18	1.49 ± 0.14	3.0 ± 5.4
$LREF_{CERWM}$	Amygdala	1.13 ± 0.10	1.15 ± 0.10	0.92	1.94	3.20	1.13 ± 0.10	1.16 ± 0.07	2.7 ± 6.8
	Cerebellum	1.18 ± 0.03	1.18 ± 0.06	0.71	0.01	2.85	1.18 ± 0.02	1.17 ± 0.04	−0.3 ± 2.0
	Frontal Lobe	1.36 ± 0.07	1.36 ± 0.07	0.59	0.51	4.49	1.41 ± 0.25	1.33 ± 0.08	−4.5 ± 11.1
	Gyrus Cinguli	1.42 ± 0.10	1.43 ± 0.09	0.77	0.48	4.52	1.44 ± 0.16	1.39 ± 0.07	−2.9 ± 8.3
	Insula	1.29 ± 0.09	1.29 ± 0.08	0.66	0.46	5.30	1.29 ± 0.11	1.26 ± 0.06	−2.1 ± 5.9
	Occipital Lobe	1.34 ± 0.08	1.34 ± 0.07	0.76	−0.29	3.59	1.33 ± 0.07	1.32 ± 0.06	−1.1 ± 3.8
	Parietal Lobe	1.36 ± 0.07	1.37 ± 0.07	0.65	1.14	4.35	1.38 ± 0.14	1.32 ± 0.06	−3.3 ± 8.2
	Striatum	1.15 ± 0.11	1.17 ± 0.09	0.88	1.55	4.00	1.14 ± 0.12	1.12 ± 0.07	−1.4 ± 6.6
	Temporal Lobe	1.27 ± 0.09	1.28 ± 0.08	0.79	0.18	4.50	1.28 ± 0.10	1.26 ± 0.08	−1.2 ± 6.6
	Thalamus	1.30 ± 0.08	1.33 ± 0.08	0.73	2.09	4.06	1.35 ± 0.06	1.32 ± 0.06	−1.9 ± 6.1
$SRTM_{CERWM}$	Amygdala	1.14 ± 0.08	1.16 ± 0.09	0.92	2.13	2.82	1.14 ± 0.10	1.17 ± 0.09	3.0 ± 8.6
	Cerebellum	1.16 ± 0.03	1.15 ± 0.05	0.70	−0.63	2.62	1.15 ± 0.02	1.15 ± 0.04	−0.1 ± 2.1
	Frontal Lobe	1.39 ± 0.07	1.38 ± 0.10	0.79	−0.90	3.82	1.44 ± 0.25	1.35 ± 0.08	−4.9 ± 10.9
	Gyrus Cinguli	1.45 ± 0.11	1.44 ± 0.12	0.87	−0.58	3.93	1.46 ± 0.16	1.40 ± 0.07	−3.6 ± 8.0
	Insula	1.30 ± 0.09	1.30 ± 0.09	0.74	−0.50	5.02	1.31 ± 0.11	1.27 ± 0.06	−2.6 ± 6.2
	Occipital Lobe	1.36 ± 0.08	1.34 ± 0.09	0.81	−1.63	3.83	1.34 ± 0.07	1.33 ± 0.07	−1.4 ± 3.8
	Parietal Lobe	1.38 ± 0.08	1.38 ± 0.10	0.78	−0.02	4.03	1.40 ± 0.15	1.34 ± 0.07	−3.7 ± 8.1
	Striatum	1.17 ± 0.10	1.18 ± 0.09	0.87	0.92	4.19	1.17 ± 0.10	1.14 ± 0.06	−1.7 ± 6.5
	Temporal Lobe	1.30 ± 0.10	1.29 ± 0.11	0.87	−1.23	4.15	1.30 ± 0.10	1.28 ± 0.08	−1.6 ± 6.4
	Thalamus	1.30 ± 0.08	1.32 ± 0.10	0.80	1.22	4.03	1.34 ± 0.06	1.32 ± 0.06	−1.9 ± 5.7

Data are presented as mean values (± SD). Data in bold indicate significant differences between sessions ($p<0.05$).

variability was slightly higher, ranging from 4.7% (cerebellum) to 7.9% (frontal lobe) with the *LREF*. Using the CERWM as reference region, the test-retest DVR variability ranged from 2.8% (cerebellum) to 5.3% (insula) with the *LREF* and from 2.6% (cerebellum) to 5% (insula) with the *SRTM*. The mean bias across all ROIs was trivial (< 4%). Of note, using *SRTM* method, the R1 parameter in any ROI was not significantly different between test and retest using the CC or the CERWM as reference tissue ($p = 1$ and $p = 0.97$ respectively).

3.5. Challenge study

There were no significant differences between test and challenge scans in neither the amount of injected radioactivity (Scan 1: 362 ± 14 MBq; Scan 2: 370 ± 13 MBq; *Student*_t_6 = −0.98; $p = 0.367$) nor the molecular activity of [^{11}C]yohimbine (Scan 1: 27.7 ± 10.9 GBq/μmol; Scan 2: 25.3 ± 7.4 GBq/μmol; *Student*_t_6 = 0.47; $p = 0.652$). The mean systolic and diastolic arterial blood pressures were 120 and 76 mmHg, respectively at the time of administration. Ninety minutes after administration, clonidine produced a transient 24% decrease only in the mean diastolic blood pressure ($\chi^2(6)$=17.81, $p = 0.007$). This effect of clonidine on the cardiovascular system is in good agreement with the literature (Talke et al., 2001). At the anatomical regional level, results of the challenge study are given in Table 4 (right part). Significant increase of DVR in the challenge compared to the baseline condition was only observed in the amygdala (+6%) and striatum (+4%) with $SRTM_{CC}$. Im-

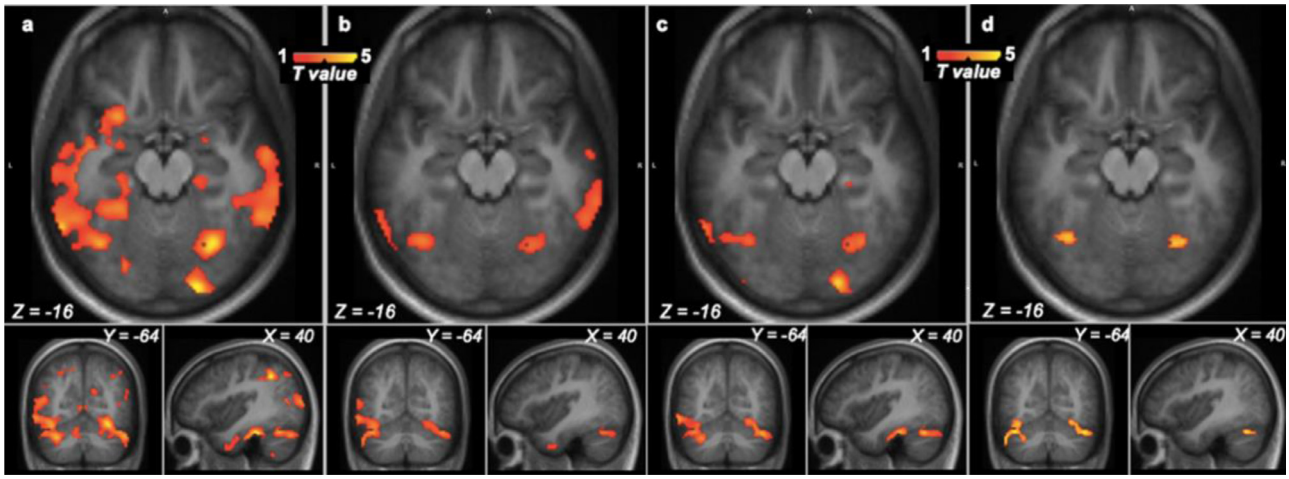

Fig. 3. MRI overlaid with t-statistic maps comparing DVR values with CC as reference region and *SRTM* method (a), *LREF* method (b), and with CERWM as reference region and *SRTM* method (c), *LREF* method (d) and obtained from SPM comparing test and challenge minus test and retest studies using height threshold of $P < 0.05$ uncorrected at the voxel level and an extent voxels threshold the "*Expected number of voxel per cluster*" (246, 427, 260 and 294 voxels respectively for (a), (b) (c) and (d) maps).

portantly, using *SRTM* method, the R1 parameter in any ROI was not significantly different between test and challenge using the CC or the CERWM as reference tissue ($p = 0.99$ and $p = 0.91$ respectively.

3.5.1. Statistical parametric mapping

Statistical parametric maps present the results of the comparison between challenge and test conditions, for the challenge group, with respect to the same comparison in test-retest control group (*t contrast* of condition effect: $(DVR_2\text{-}DVR_1)_{Challenge} - (DVR_2\text{-}DVR_1)_{control}$). Fig. 3 shows the thresholded maps for the $SRTM_{CC}$ (3a), the $LREF_{CC}$ (3b), and the $SRTM_{CERWM}$ (3c), and the $LREF_{CERWM}$ (3d).

Table 5 gives the cluster parameters that elicited differences according to the parametric imaging method (*SRTM* or *LREF)* and the reference region (CC or CERWM). Using *SRTM* and the CC, two clusters showed significant activities including bilaterally the temporal and occipital fusiform gyrus, the cerebellum, the lateral part of the occipital cortex, the middle temporal gyrus, as well as the right occipital pole, inferior temporal gyrus and angular gyrus. Same contrast with *SRTM* and the CERWM reference region or with the *LREF* model did not show any significant cluster. Yet, these contrasts showed activities mainly located in the posterior part of the brain encompassing the temporal and occipital cortex as well as the cerebellum, as observed significantly using the $SRTM_{CC}$ imaging method.

4. Discussion

The regional distribution of [^{11}C]yohimbine binding corresponds with the known distribution of α2-ARs in post mortem human brain studies (Ordway et al., 1993; Vos et al., 1992). The most prominent uptake of the tracer was seen in cortical brain regions, especially in the cingulum, frontal, parietal and occipital cortices whereas uptake was less prominent in the striatum and the cerebellum (Fig. 4).

4.1. The kinetic modeling study

In order to evaluate a reliable and suitable method for α2-ARs quantification, we compared various invasive and non-invasive models, often used for brain receptor quantification.

Using invasive models and direct fitting of the PET kinetics with tissue compartmental model and AIF, the 1-TCM was found to be sufficient for describing the tracer kinetics of [^{11}C]yohimbine in the healthy human brain (Nahimi et al., 2015). Testing the LGA alternative to 1-TCM as a simpler resolution method from an algorithmic point of view led to results quite similar despite a very limited higher V_T values found with LGA (around 12%). This might be attributed to the fact that blood volume, Vb, is not taken into account in LGA model. However, since Vb is fairly stable over the regions, this overestimation does not exclude the use of LGA as an alternative method to 1-TCM for a reliable estimate of the volume of distribution.

With non-invasive models, our findings show, for the first time, the feasibility of using a simple acquisition protocol for kinetic modeling avoiding arterial blood sampling. In particular, DVR estimated using non-invasive kinetic models (*LREF* and *SRTM*) showed an excellent correlation to the invasive 1-TCM whatever the reference region (CC, CERWM or FLWM) with the best fit obtained for $SRTM_{CC}$ (R^2=0.94). Of note, the results indicated a slight tendency toward an overestimation with CC (slope equal to 1.07 using LREF and 1.13 with SRTM). However, since the correlation with the 1-TCM is excellent and stable across brain regions, the induced bias can be predicted and should not have an impact on comparative studies. In parallel, tendency toward a slight underestimation was reported with CERWM and FLWM, which was more pronounced with *SRTM* (slope equal to 0.81 and 0.94 respectively) than *LREF* (slope equal to 0.94 and 0.98 respectively). Using reference tissue methods with cerebral regions, underestimation of DVR values can be explained by a possible specific binding within the reference region as well as spill-over effect (Salinas et al., 2015). Nonetheless, CERWM or FLWM are valuable reference regions in the event of the impossibility of using the CC due to lesion of this zone in a patient, for instance.

4.2. Test-Retest reproducibility

In addition to the accuracy of the reference tissue methods, we evaluated their test-retest performance. Using FLWM as reference region, our results showed poor test-retest reliability of DVR measurements with both parametric imaging methods. However, the *SRTM* with the CERWM as reference region showed excellent test-retest reproducibility of DVR measurements, with variability ranging from 2.6% to 5.0% and a small negative bias (−0.1%). Using the *SRTM* with the CC, test-retest reproducibility of DVR measurements were a bit more spread, with a slightly higher variability ranging from 2.6% to 7.0% and a slightly higher negative bias (2%). Of importance, whatever the reference region, R_1 values, also computed with *SRTM,* did not differ between test and retest across all ROIs. In addition, the *LREF* method showed comparable very good test-retest reliability of DVR measurements (ICC=0.75) for both reference region with a slightly lower variability when using the CERWM (~ 4%) compared to the CC (~ 6%). This demonstration of

Table 5
Increase of [^{11}C]yohimbine induced by clonidine administration compared to baseline (SPM analysis).

Areas	BA	Side	MNI coordinates x	y	z	T value	P corr cluster	Cluster size
SRTM$_{CC}$								
Posterior Temporal Fusiform Cortex	20	R	42	−34	−26	6.28	0.001	6944
Cerebellum_VI	–	R	26	−48	−30	5.93		
Occipital Pole	18	R	20	−92	−16	5.14		
Angular Gyrus	40	R	38	−50	42	5.01		
Inferior Temporal Gyrus	20	R	64	−40	−20	4.91		
Occipital Fusiform Gyrus	19	R	30	−64	−16	4.67		
Cerebellum_Crus 1	–	R	56	−68	−32	4.64		
Lateral Occipital Cortex	19	R	28	−74	26	3.99		
Middle Temporal Gyrus	20	R	68	−24	−24	3.91		
Middle Temporal Gyrus	37	L	−60	−56	−12	6.15	0.001	7327
Temporal Occipital Fusiform Cortex	37	L	−32	−46	−12	5.84		
Lateral Occipital Cortex	19	L	−46	−84	12	5.55		
Cerebellum_VI	–	L	−28	−40	−30	4.51		
Cerebellum_V	–	L	−22	−36	−30	4.43		
Lateral Occipital Cortex	19	L	−52	−76	−2	4.24		
Cerebellum_Crus 1	–	L	−38	−66	−28	4.19		
Cerebellum_VIIb		L	−20	−76	−52	4.17		
Occipital Fusiform Gyrus	19	L	−38	−66	−18	3.99		
Amygdala	–	*R*	*26*	*−4*	*−20*	*3.46*	*0.970*	*271*
Parahippocampal Gyrus	*36*	*R*	*26*	*−16*	*−22*	*3.03*		
LREF$_{CC}$								
Inferior Temporal Gyrus	*20*	*R*	*64*	*−40*	*−20*	*4.71*	*0.979*	*710*
Middle Temporal Gyrus	*21*	*R*	*60*	*−10*	*−20*	*2.61*		
Lateral Occipital Cortex	*19*	*L*	*−50*	*−76*	*−4*	*4.44*	*0.979*	*1197*
Lateral Occipital Cortex	*19*	*L*	*−48*	*−82*	*10*	*4.31*		
Middle Temporal Gyrus	*37*	*L*	*−60*	*−58*	*−10*	*3.93*		
Cerebellum_Crus 1	–	*L*	*−40*	*−66*	*−26*	*3.83*		
Occipital Fusiform Gyrus	*37*	*L*	*−38*	*−64*	*−18*	*3.13*		
Cerebellum_Crus 1	–	*R*	*44*	*−62*	*−26*	*3.32*	*0.979*	*556*
Lateral Occipital Cortex	*19*	*R*	*26*	*−66*	*−16*	*2.67*		
Cerebellum_VI	–	*R*	*34*	*−64*	*−20*	*2.49*		
Cerebellum_Crus 1	–	*R*	*34*	*−74*	*−26*	*2.34*		
SRTM$_{CERWM}$								
Middle Temporal Gyrus	*37*	*L*	*−60*	*−58*	*−12*	*4.72*	*0.714*	*1718*
Lateral Occipital Cortex	*19*	*L*	*−46*	*−84*	*12*	*4.46*		
Cerebellum_VIIb	–	*L*	*−22*	*−70*	*−52*	*3.44*		
Lateral Occipital Cortex	*19*	*L*	*−52*	*−72*	*−2*	*3.44*		
Cerebellum_Crus 1	–	*L*	*−40*	*−62*	*−24*	*3.24*		
Occipital Pole	*18*	*R*	*18*	*−90*	*−14*	*4.59*	*0.971*	*1084*
Cerebellum_Crus 1	–	*R*	*44*	*−60*	*−28*	*4.55*		
Cerebellum_Crus 1	–	*R*	*32*	*−72*	*−28*	*3.19*		
Lateral Occipital Cortex	*19*	*R*	*26*	*−64*	*−12*	*3.07*		
Posterior Temporal Fusiform Cortex	*20*	*R*	*42*	*−34*	*−26*	*4.59*	*0.971*	*284*
Fusiform Gyrus	*20*	*R*	*32*	*−30*	*−26*	*3.60*		
LREF$_{CERWM}$								
Cerebellum Crus 1	–	*L*	*−52*	*−66*	*−34*	*3.38*	*0.973*	*320*
Cerebellum Crus 1	–	*L*	*−40*	*−66*	*−26*	*3.08*		
Temporal Occipital Fusiform Cortex	*37*	*L*	*−36*	*−62*	*−16*	*2.52*		
Cerebellum_Crus 1	–	*R*	*42*	*−62*	*−26*	*3.18*	*0.973*	*332*
Lateral Occipital Cortex	*19*	*R*	*26*	*−66*	*−14*	*2.96*		
Cerebellum_VI	–	*R*	*34*	*−64*	*−24*	*2.50*		

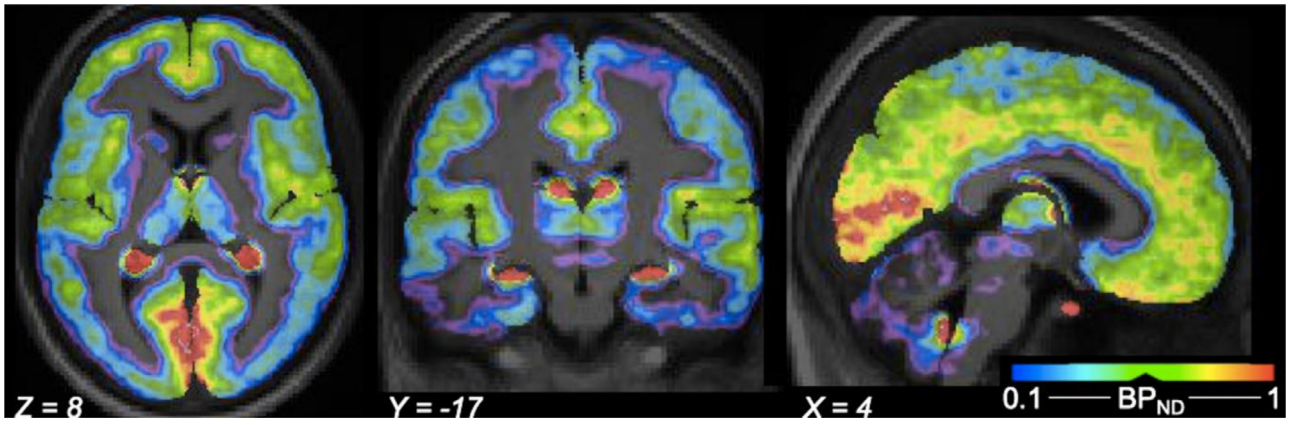

Fig. 4. Average parametric images of BP_{ND} values estimated with CC as reference region and *SRTM* method overlaid on the mean MRI images of the 14 participants during the first scan. Color bar gives estimates of BP_{ND} in units of $mL.cm^{-3}$.

a reproducible [^{11}C]yohimbine PET outcome measure using CERWM or CC is critical for further clinical investigations in larger studies.

4.3. Challenge study

So far, very limited evidence has been presented to support PET imaging of noradrenaline neurotransmission in humans. The brain uptake and receptor binding of [^{11}C]yohimbine was found to be reduced by unlabeled yohimbine challenge, amphetamine administration or by acute vagus nerve stimulation in rats and/or Landrace pig brain (Jakobsen et al., 2006; Landau et al., 2015, 2012; Phan et al., 2017, 2015).

In our study, regional analyses showed significant regional change induced by the challenge with clonidine within the amygdala and the striatum, only when using the *SRTM* with the CC as reference region. In parallel, we conducted a voxel-based analysis as this latter has several advantages over the ROI-based approach, including the use of SPM to identify alterations in receptor binding in all brain areas without anatomical *a priori*. Interestingly, the voxel-based analysis showed changes that were not discernable with the ROIs analysis, where delineation of regions is determinist and based on anatomo-functional considerations. In particular, statistical parametric maps of [^{11}C]yohimbine binding under clonidine administration showed significant specific increases in the posterior part of the brain including the temporal and occipital lobes, as well as the cerebellum. However, this increase was again reported only when using *SRTM* with the CC as reference region. Overall, the pattern of increased [^{11}C]yohimbine uptake observed with this voxel-based analysis is consistent with previous studies demonstrating that α2-ARs agonists changed regional cerebral blood flow (CBF) in posterior cortical regions including the cerebellum, the temporal cortex and the angular gyrus (Bonhomme et al., 2008; Fu et al., 2001). This increase in [^{11}C]yohimbine binding is likely the consequence of clonidine acting at presynaptic α2-ARs sites resulting in reduced noradrenergic neurotransmission (Dennis et al., 1987; Starke, 1981) and leading to a state of low tonic arousal. Indeed, all of our volunteers reported that time spent in the scanner during the challenge condition had seemed shorter than during the first baseline scan. Considering the known effect of clonidine on vigilance (Coull et al., 2004; Hall et al., 2001), we can reasonably assume that our participants had a low level of consciousness during the challenge scan. Interestingly, many studies have previously highlighted the role of a posterior network in the deleterious effect of clonidine on attention and arousal (Bonhomme et al., 2008; Coull et al., 2004; Fu et al., 2001). In particular, the results of the present study reinforce the nonmotor role of the cerebellum (Strick et al., 2009) through α2-ARs modulation (Schambra et al., 2005) as well as the role of the fusiform gyrus and lateral occipital cortex in attention (Tallon-Baudry et al., 2005).

4.4. Limitations of the study

There are some limitations in this study that has to be mentioned. First, the experimental design did not provide for arterial blood sampling during the second scan session. In fact, the first objective of the present study was to validate the use of a simplified reference tissue model, and the second objective was to assess both the reproducibility and the sensitivity of [^{11}C]yohimbine PET measurements estimated with this simplified modeling method. To this end, we limited the use of the invasive sampling of arterial blood only to the first scan in order not to lose volunteers for the second scan who might not want to repeat this unpleasant experience. Yet, it would have made sense to have arterial input in the clonidine challenge to evaluate the impact of the challenge on peripheral metabolism, if any, as well as to quantify the true volume of non-displaceable volume of distribution in the potential reference regions. This point would merit further investigations. Then, another shortcoming is the proportion of clonidine that bounds to plasma protein. Indeed, free plasma fraction can change upon pharmacological challenge due to displacement of ligand binding to plasma proteins. For instance, Phan et al. (2017) have shown an elevation of *fp* in response to challenge with unlabeled yohimbine. However, it has to be highlighted that the bound fraction of yohimbine to plasma proteins is around 80% (Berlan et al., 1993) while this bound fraction for clonidine is register to be of 20% (Khan et al., 1999). Although we cannot completely rule out the possibility of a change of *fp* upon clonidine challenge, we believe this is very unlikely since the reported protein binding is relatively low. Indeed, within the same range (around 20%, (de la Torre et al., 2004) no change of *fp* has been observed with amphetamine challenge (Phan et al., 2015). In the same vein, the potential effects of clonidine on CBF should also be considered. Since [^{11}C]yohimbine was administered as a systemic bolus, potential changes in CBF might affect the kinetics of the tracer in the brain and influence its binding. In humans, clonidine is known to decrease blood pressure and reduce CBF (James et al., 1970; Lee et al., 1997). In our study, administration of clonidine produced a transient 26% decrease in mean diastolic arterial blood pressure. A clonidine-induced decrease in CBF could decrease the delivery of the tracer, which would induce a smaller Vt, therefore an underestimation of the clonidine-induced increase in α2-ARs binding. In other terms, the effect of clonidine in the present study, might have been underestimated. Finally, the results of the present study cannot completely rule out a possible effect of genotype (see supplementary materials). Further studies are needed to confirm this observation. In the meantime, the authors recommend to genotype volunteers for the cytochrome P450 system with regard to the CYP2D6 isoform if between groups comparisons have to be performed.

Conclusion

Our results support the use of [^{11}C]yohimbine PET in the in vivo assessment of human brain α2-ARs. Rapid tracer uptake associated with low test-retest variability and good reproducibility was demonstrated in the regions with the highest densities of the α2-ARs. In particular, the authors recommend the use of [^{11}C]yohimbine parametric imaging of DVR by non-invasive *SRTM* using the CC as reference tissue for imaging α2-ARs. This method was able to evidence moderate occupancy with concurrent drug on α2-ARs. Alternatively, CERWM might be considered when measurements in the CC would not be reliable for structural or lesional reason. In other terms, simplified imaging protocols can be used for reliable [^{11}C]yohimbine PET quantification which opens the possibility to investigate, in large human samples, the role of α2-ARs in various neuropsychiatric disorders including schizophrenia, depression, Parkinson's disease and Alzheimer's disease.

Declaration of Competing Interest

The authors have no conflicts of interest to declare that are relevant to the content of this article.

Acknowledgments

We thank the healthy volunteers who participated in this trial. We thank Dr Gagnieu MC and her team for the genotyping analyses (HCL, UM Pharmacology-Toxicology).

Funding

This work was supported by the french national 'invest for the futur' programs (LILI – Lyon Integrated Life Imaging: hybrid MR-PET ANR-11-EQPX-0026); and the French "Agence Nationale pour la Recherche" (ANR-16-CE37-0014). ZI is partially supported by Siemens-Heathcare SAS.

Data/code availability statement

Public access to the data online is not permitted without the approval of the study's sponsor namely the Hospices Civils de Lyon (Protocol ID 69HCL17_0196). The authors will be happy to support request for a formal data sharing agreement.

Supplementary materials

Supplementary material associated with this article can be found, in the online version, at doi:10.1016/j.neuroimage.2021.118328.

References

Akaike, H., 1974. A new look at the statistical model identification. IEEE Trans. Automat. Contr. 19, 716–723. doi:10.1109/TAC.1974.1100705.

Ashburner, J., Friston, K.J., 2005. Unified segmentation. Neuroimage 26, 839–851. doi:10.1016/j.neuroimage.2005.02.018.

Bonhomme, V., Maquet, P., Phillips, C., Plenevaux, A., Hans, P., Luxen, A., Lamy, M., Laureys, S., 2008. The effect of clonidine infusion on distribution of regional cerebral blood flow in volunteers. Anesthes. Analges. 106, 899–909. doi:10.1213/ane.0b013e3181619685.

Coull, J.T., Jones, M.E.P., Egan, T.D., Frith, C.D., Maze, M., 2004. Attentional effects of noradrenaline vary with arousal level: selective activation of thalamic pulvinar in humans. Neuroimage 22, 315–322. doi:10.1016/j.neuroimage.2003.12.022.

de la Torre, R., Farré, M., Navarro, M., Pacifici, R., Zuccaro, P., Pichini, S., 2004. Clinical pharmacokinetics of amfetamine and related substances: monitoring in conventional and non-conventional matrices. Clin. Pharmacokinet. 43, 157–185. doi:10.2165/00003088-200443030-00002.

Delaville, C., Deurwaerdère, P.D., Benazzouz, A., 2011. Noradrenaline and Parkinson's disease. Front. Syst. Neurosci. 5. doi:10.3389/fnsys.2011.00031.

Dennis, T., L'Heureux, R., Carter, C., Scatton, B., 1987. Presynaptic alpha-2 adrenoceptors play a major role in the effects of idazoxan on cortical noradrenaline release (as measured by in vivo dialysis) in the rat. J. Pharmacol. Exp. Ther. 241, 642–649.

Fu, C.H.Y., Reed, L.J., Meyer, J.H., Kennedy, S., Houle, S., Eisfeld, B.S., Brown, G.M., 2001. Noradrenergic dysfunction in the prefrontal cortex in depression: an [15O] H2O PET study of the neuromodulatory effects of clonidine. Biol. Psychiatry 49, 317–325. doi:10.1016/S0006-3223(00)01050-7.

Gunn, R.N., Lammertsma, A.A., Hume, S.P., Cunningham, V.J., 1997. Parametric imaging of ligand-receptor binding in pet using a simplified reference region model. Neuroimage 6, 279–287. doi:10.1006/nimg.1997.0303.

Hall, J.E., Uhrich, T.D., Ebert, T.J., 2001. Sedative, analgesic and cognitive effects of clonidine infusions in humans †. Br. J. Anaesth. 86, 5–11. doi:10.1093/bja/86.1.5.

Hammers, A., Allom, R., Koepp, M.J., Free, S.L., Myers, R., Lemieux, L., Mitchell, T.N., Brooks, D.J., Duncan, J.S., 2003. Three-dimensional maximum probability atlas of the human brain, with particular reference to the temporal lobe. Hum. Brain Mapp. 19, 224–247. doi:10.1002/hbm.10123.

Heckemann, R.A., Keihaninejad, S., Aljabar, P., Rueckert, D., Hajnal, J.V., Hammers, A., 2010. Improving intersubject image registration using tissue-class information benefits robustness and accuracy of multi-atlas based anatomical segmentation. Neuroimage 51, 221–227. doi:10.1016/j.neuroimage.2010.01.072.

Jakobsen, S., Pedersen, K., Smith, D.F., Jensen, S.B., Munk, O.L., Cumming, P., 2006. Detection of α2-Adrenergic Receptors in Brain of Living Pig with 11C-Yohimbine. J. Nucl. Med. 47 2008–2015.

James, I.M., Larbi, E., Zaimis, E., 1970. The effect of the acute intravenous administration clonidine (St 155) on cerebral blood flow in man. Br. J. Pharmacol. 39, 198P–199P.

Khan, Z.P., Ferguson, C.N., Jones, R.M., 1999. Alpha-2 and imidazoline receptor agonists-Their pharmacology and therapeutic role: alpha-2 and imidazoline receptor agonists. AnaesthesiaAnaesthesia 54, 146–165. doi:10.1046/j.1365-2044.1999.00659.x.

Lammertsma, A.A., Hume, S.P., 1996. Simplified reference tissue model for PET receptor studies 4, 153–158.

Landau, A.M., Doudet, D.J., Jakobsen, S., 2012. Amphetamine challenge decreases yohimbine binding to α2 adrenoceptors in Landrace pig brain. Psychopharmacology (Berl.) 222, 155–163. doi:10.1007/s00213-011-2632-6.

Landau, A.M., Dyve, S., Jakobsen, S., Alstrup, A.K.O., Gjedde, A., Doudet, D.J., 2015. Acute vagal nerve stimulation lowers α2 adrenoceptor availability: possible mechanism of therapeutic action. Brain Stimul. 8, 702–707. doi:10.1016/j.brs.2015.02.003.

Le Corre, P., Dollo, G., Chevanne, F., Le Verge, R., 1999. Biopharmaceutics and metabolism of yohimbine in humans. Eur. J. Pharm. Sci. 9, 79–84. doi:10.1016/S0928-0987(99)00046-9.

Lee, H.W., Caldwell, J.E., Dodson, B., Talke, P., Howley, J., 1997. The effect of clonidine on cerebral blood flow velocity, carbon dioxide cerebral vasoreactivity, and response to increased arterial pressure in human volunteers. Anesthesiology 87, 553–558. doi:10.1097/00000542-199709000-00015.

Logan, J., 2000. Graphical analysis of PET data applied to reversible and irreversible tracers. Nucl. Med. Biol. 27, 661–670. doi:10.1016/S0969-8051(00)00137-2.

Marien, M.R., Colpaert, F.C., Rosenquist, A.C., 2004. Noradrenergic mechanisms in neurodegenerative diseases: a theory. Brain Res. Rev. 45, 38–78. doi:10.1016/j.brainresrev.2004.02.002.

Mérida, I., Reilhac, A., Redouté, J., Heckemann, R.A., Costes, N., Hammers, A., 2017. Multi-atlas attenuation correction supports full quantification of static and dynamic brain PET data in PET-MR. Phys. Med. Biol. 62, 2834–2858. doi:10.1088/1361-6560/aa5f6c.

Millan, M.J., Newman-Tancredi, A., Audinot, V., Cussac, D., Lejeune, F., Nicolas, J.P., Cogé, F., Galizzi, J.P., Boutin, J.A., Rivet, J.M., Dekeyne, A., Gobert, A., 2000. Agonist and antagonist actions of yohimbine as compared to fluparoxan at alpha(2)-adrenergic receptors (AR)s, serotonin (5-HT)(1A), 5-HT(1B), 5-HT(1D) and dopamine D(2) and D(3) receptors. Significance for the modulation of frontocortical monoaminergic transmission and depressive states. Synapse 35, 79–95. doi:10.1002/(SICI)1098-2396(200002)35, 2<79::AID-SYN1>3.0.CO;2-X.

Moore, A.E.B., Hain, S.F., Blake, G.M., Fogelman, I., 2003. Validation of ultrafiltration as a method of measuring free 99mTc-MDP 44, 891–897.

Nahimi, A., Jakobsen, S., Munk, O.L., Vang, K., Phan, J.A., Rodell, A., Gjedde, A., 2015. Mapping 2 adrenoceptors of the human brain with 11C-yohimbine. J. Nucl. Med. 56, 392–398. doi:10.2967/jnumed.114.145565.

Ordway, G.A., Jaconetta, S.M., Halaris, A.E., 1993. Characterization of subtypes of alpha-2 adrenoceptors in the human brain. J. Pharmacol. Exp. Ther. 264, 967–976.

Ordway, G.A., Schenk, J., Stockmeier, C.A., May, W., Klimek, V., 2003. Elevated agonist binding to alpha-2-adrenoceptors in the locus coeruleus in major depression. Biol. Psychiatry 53, 9.

Phan, J.-A., Landau, A.M., Jakobsen, S., Wong, D.F., Gjedde, A., 2017. Radioligand binding analysis of α2 adrenoceptors with [11C]yohimbine in brain in vivo: extended Inhibition Plot correction for plasma protein binding. Sci. Rep. 7. doi:10.1038/s41598-017-16020-1.

Phan, J.-A., Landau, A.M., Wong, D.F., Jakobsen, S., Nahimi, A., Doudet, D.J., Gjedde, A., 2015. Quantification of [^{11}C]yohimbine binding to α_2 adrenoceptors in rat brain in vivo. J. Cereb. Blood Flow Metab. 35, 501–511. doi:10.1038/jcbfm.2014.225.

Poline, J.-B., Worsley, K.J., Evans, A.C., Friston, K.J., 1997. Combining spatial extent and peak intensity to test for activations in functional imaging. Neuroimage 5, 83–96. doi:10.1006/nimg.1996.0248.

Reilhac, A., Merida, I., Irace, Z., Stephenson, M.C., Weekes, A.A., Chen, C., Totman, J.J., Townsend, D.W., Fayad, H., Costes, N., 2018. Development of a dedicated rebinner with rigid motion correction for the mMR PET/MR scanner, and validation in a large cohort of 11C-PIB Scans 59, 1761–1767.

Salinas, C.A., Searle, G.E., Gunn, R.N., 2015. The Simplified Reference Tissue Model: model Assumption Violations and Their Impact on Binding Potential. J. Cereb. Blood Flow Metab. 35, 304–311. doi:10.1038/jcbfm.2014.202.

Schambra, U.B., Mackensen, G.B., Stafford-Smith, M., Haines, D.E., Schwinn, D.A., 2005. Neuron specific α-adrenergic receptor expression in human cerebellum: implications for emerging cerebellar roles in neurologic disease. Neuroscience 135, 507–523. doi:10.1016/j.neuroscience.2005.06.021.

Shrout, P.E., Fleiss, J.L., 1979. Intraclass correlations: uses in assessing rater reliability 86, 420–428.

Starke, K., 1981. Alpha-adrenoceptor sub-classification. Rev. Physiol. Biochem. Pharmacol. 88, 199–236.

Strick, P.L., Dum, R.P., Fiez, J.A., 2009. Cerebellum and nonmotor function. Annu. Rev. Neurosci. 32, 413–434. doi:10.1146/annurev.neuro.31.060407.125606.

Szabadi, E., 2013. Functional neuroanatomy of the central noradrenergic system. J. Psychopharmacol. 27, 659–693. doi:10.1177/0269881113490326.

Talke, P.O., Lobo, E.P., Brown, R., Richardson, C.A., 2001. Clonidine-induced vasoconstriction in awake volunteers. Anesth. Analg. 6.

Tallon-Baudry, C., Bertrand, O., Hénaff, M.-A., Isnard, J., Fischer, C., 2005. Attention modulates gamma-band oscillations differently in the human lateral occipital cortex and fusiform gyrus. Cereb. Cortex 15, 654–662. doi:10.1093/cercor/bhh167.

Varga, J., Szabo, Z., 2002. Modified regression model for the logan plot. J. Cereb. Blood Flow Metab. 22, 240–244. doi:10.1097/00004647-200202000-00012.

Vos, H., Vauquelin, G., Keyser, J., Backer, J.-P., Liefde, I., 1992. Regional distribution of ? $_{2A}$ -and ? $_{2B}$ -adrenoceptor subtypes in postmortem human brain. J. Neurochem. 58, 1555–1560. doi:10.1111/j.1471-4159.1992.tb11378.x.